ARTICLE

Generation of Nanoparticles of Controlled Size Using Ultrasonic Piezoelectric Oscillators in Solution

Ian K. Wright,*,† Andrew Higginbotham,† Shenda M. Baker,‡ and T. D. Donnelly†

Department of Physics and Department of Chemistry, Harvey Mudd College, 301 Platt Boulevard, Claremont, California 91711

ABSTRACT We demonstrate the operation of a device that can produce chitosan nanoparticles in a tunable size range from 50−300 nm with small size dispersion. A piezoelectric oscillator operated at megahertz frequencies is used to aerosolize a solution containing dissolved chitosan. The solvent is then evaporated from the aerosolized droplets in a heat pipe, leaving monodisperse nanoparticles to be collected. The nanoparticle size is controlled both by the concentration of the dissolved polymer and by the size of the aerosol droplets that are created. Our device can be used with any polymer or polymer/therapeutic combination that can be prepared in a homogeneous solution and vaporized.

KEYWORDS: piezoelectric oscillators • chitosan • nanoparticles • atomization • nebulizers • nanopolymers

INTRODUCTION

Nanoparticles have found increasing usefulness as biomedical tools (1). Gold nanoparticles, for instance, are now commonly used in many types of imaging, as they are highly scattering yet are small enough to not interfere with the chemistry and biology of the samples being studied (2). Nanoparticles are also finding more subtle and sophisticated roles as our ability to control their size improves. In medical applications, for example, they can be used as carriers for gene therapy or drug delivery.

Gene therapy has recently emerged as a promising tool to help treat a variety of diseases, including many otherwise untreatable types of cancer and neurodegenerative conditions (3). The greatest challenge for this technology has proved to be finding methods to safely deliver the genes to the target cells with high specificity, biocompatibility, and controlled delivery. Viruses have been the most commonly used vectors for this delivery, but potentially life threatening immune reactions and unclear safety profiles in the host have limited their use (4).

Because of the safety concerns surrounding viral-vectors, polymeric nanoparticles are being developed to encapsulate and deliver therapeutic genes. Depending on their size, charge, and composition, nanoparticles can be targeted to specific tissues, as fenestrations in the vasculature vary in size. Individual cell and tissue types also take up nanoparticles to different degrees, depending on the particle size (5). For further cell specificity, attaching specific ligands to the surface of nanoparticles has been heavily researched and can be used to target leukemic and other harmful cells (6).

Similar benefits also apply to using nanoparticles for drug delivery. As in gene therapy, therapeutic drugs are typically tissue specific and targeted delivery allows for a higher dose of the drugs to be delivered only to tissues where they are needed, improving disease resolution as well as minimizing potential side effects (7). For both transfection of genes and delivering drugs into cells, the delivery rate affects both how long the therapy interacts with the system and its efficacy and toxicity (8, 9). The polymers comprising the nanoparticles can be modulated to control the rate, location, pH, or delay of delivery. In vaccine development, antigens can be protected by the nanoparticles and delivered specifically to the lymphoid system where they can promote a productive immune response (10).

As the size of the nanoparticles produced greatly affects their rate of cellular uptake, as well as their longevity in vivo, a variety of methods have been developed that attempt to produce monodisperse nanoparticles of desired sizes, including techniques such as emulsification and solvent evaporation (7, 11−13). However, because each of the methods currently used in nanoparticle production relies on the physical properties of the polymer and the therapeutic drugs with which it will be formulated, these techniques are limited and must be modified for any change in molecular weight, dose, ionic strength, pH, etc.

In contrast to these methodologies, we have developed a device which uses a novel and generally applicable method of generating narrowly disperse nanoparticles of sizes optimal for cellular uptake (50−300 nm) that could be used to efficiently incorporate a variety of drugs. As a proof of concept we have created chitosan nanoparticles, as they are

* Corresponding author. E-mail: ikwright@gmail.com.
Received for review April 28, 2010 and accepted July 7, 2010
† Department of Physics, Harvey Mudd College.
‡ Department of Chemistry, Harvey Mudd College.
DOI: 10.1021/am100375w

Published on Web 07/20/2010

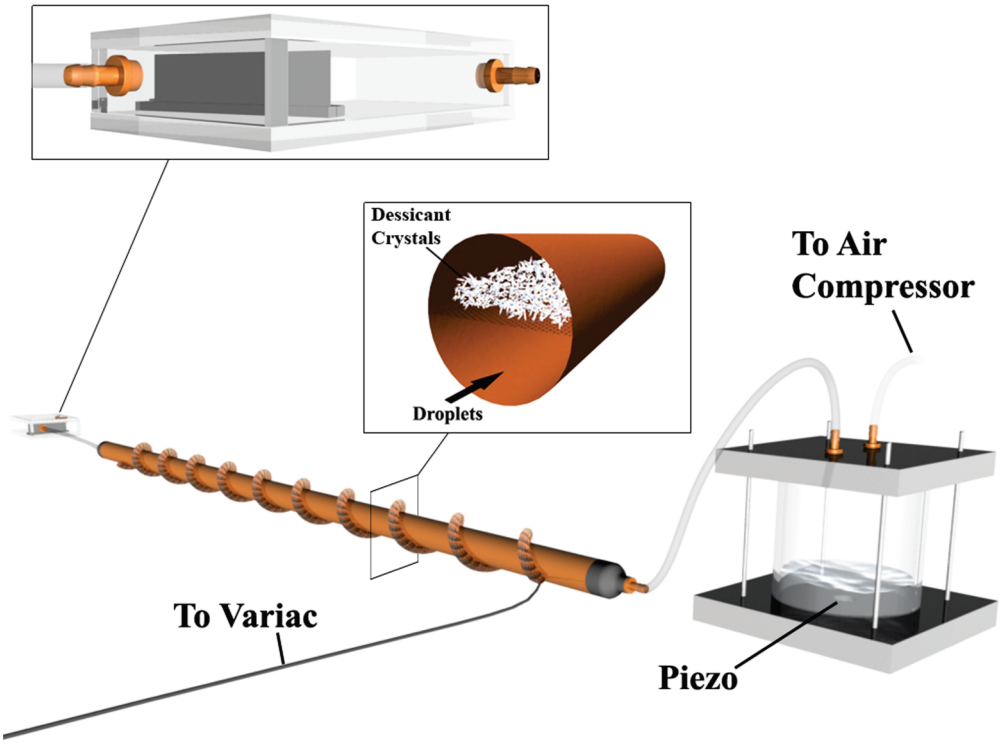

FIGURE 1. Experimental setup used to generate chitosan nanoparticles. The aqueous chitosan solution was added to the cylindrical container and driven by a high-frequency piezoelectric, which aerosolized the solution. Following aerosolization, the droplets were blown through the hot, dry environment of the copper pipe, where the solvent was evaporated, leaving only the nanoparticles. These particles were then carried to the location of collecting slides. Vinyl tubing (shown as clear) was used to connect the various parts of the setup.

particularly relevant to medical treatments; the methods we describe, however, are generally applicable to any soluble polymer.

METHODS

To produce chitosan nanoparticles, we first generated droplets from a chitosan solution contained within a cylindrical chamber (see Figure 1). This atomization was achieved by placing a piezoelectric oscillator at the bottom of the chamber, which was driven using less than 10 W. Once the droplets were formed, an air compressor was used to direct them into a vinyl tube connected to a 6 foot long, 1.125 in. diameter copper pipe. Heat tape was wrapped helically along the length of the pipe, which induced the solvent to evaporate off of the droplets, generating chitosan nanoparticles. This process was further enhanced by placing Drierite crystals in the last 2 feet of pipe, suspended in the top half by a wire mesh. These crystals were important in absorbing excess moisture in the tube, accelerating the evaporation process, and ensuring the nanoparticles were successfully dried. The exit of this pipe was then connected to a collection chamber, in which a silicon slide was placed upright. Nanoparticles exiting the pipe impacted this slide, and could then be visualized directly using a scanning electron microscope.

Our method of creating nanoparticles of a specific size is conceptually straightforward. A solution of the target polymer is prepared at a known concentration, after which it is atomized to create an aerosol of droplets of a well-known size. Provided that the droplet size and the solution concentration are known, the quantity of polymer contained in each droplet can easily be determined. The droplets are then sent through the controlled environment of a heat pipe, thus evaporating the solvent and leaving only the residual polymer contained in the original droplet. The residual polymer clumps together to form a nanoparticle, and is then collected.

The technical challenge in this method is creating a dense aerosol containing droplets of a uniform size, as the dispersion

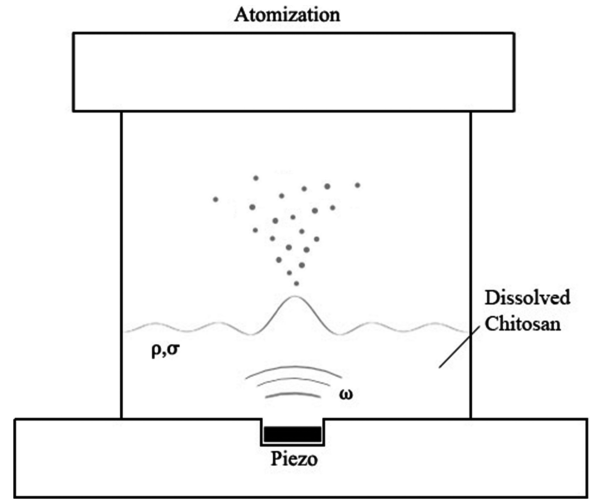

FIGURE 2. Schematic for the production of nanoparticles. In the aerosolization chamber, a piezo oscillates at frequency ω, creating pressure waves in the fluid. Depending on the fluid's density ρ and surface tension σ, droplets of a particular diameter are ejected. The droplets contain some of the dissolved chitosan, which forms nanoparticles when the solvent is evaporated.

in droplet size is directly related to the variability in nanoparticle size. We use ultrasonic atomization to create such an aerosol. Our methods are described in detail in refs 14 and 15, and we summarize them here.

Aerosols are created using the apparatus shown in Figure 2. A piezoelectric (piezo) oscillating at megahertz frequencies is placed at the bottom of the fluid containing dissolved chitosan, thereby generating Faraday waves at the fluid surface. If these surface waves are driven strongly enough by the piezo, then droplets will be ejected from the fluid surface. Models show that the size of droplets produced by excitation of the fluid surface

is related to the oscillation frequency of the piezo and the properties of the fluid. The relationship between droplet size and the fluid parameters breaks down into two regimes of phase-space: the inviscid (low driving frequency, surface tension-dominated) and viscous (high driving frequency, viscosity-dominated). As we operated in the inviscid regime of droplet formation (the kinematic viscosity having no effect on droplet size), the droplet diameter, d, is given by

$$d = 2\pi c\left(\frac{\sigma}{\rho}\right)^{1/3}\left(\frac{2}{\omega}\right)^{2/3} \quad (1)$$

where σ is surface tension, ρ is density, ω is the frequency at which the fluid is driven, and c is a constant that we have measured to be $c = 0.35 \pm 0.03$. For a particular sample fluid, therefore, the primary determinant of droplet size is the driving frequency of the piezo, both because of the weak power law dependence of the surface tension and density, and because most fluids of interest have similar values for these parameters.

Another factor that could potentially affect the size of the droplets produced is the amplitude of the piezo oscillations. However, we have determined both experimentally and theoretically that this value is only important if the piezo is driven outside of the subharmonic regime of the Faraday instability (well-above the threshold driving power required to produce droplets). Instead, we drove the fluid relatively near the threshold power for atomization, which ensures that we remained in the subharmonic regime where the particle size is relatively insensitive to the driving power. If, by some error, we had driven the fluid to the point that we were exciting harmonic Faraday waves, and thus created undersized droplets, the evidence of this would have been a population of chitosan nanoparticles that were roughly 1/8th the size of the larger population, which was not observed.

From eq 1, one can therefore determine how to make droplets of a desired size: For a given sample, fluid properties are measured and then the sample is driven at an appropriate frequency to produce a droplet of the specified size. For example, at room temperature, water has fluid property values of $\sigma = 0.073$ N/m, $\rho = 997$ kg/m^3, $\nu = 1.0 \times 10^{-6}$ m^2/s. To make a droplet with $d = 1$ μm, therefore, the fluid must be driven at frequency $f = \omega/2\pi = 8.5$ MHz.

In the device described here, we use piezos operating at 6.6 and 2.4 MHz to create nanoparticles. We also limited the power input to 10 W, as this minimized the temperature change of the solution. Too much of a temperature increase might otherwise alter the surface tension and thus the size of the droplets produced, though this effect would likely be minimal given the weak power law dependence (see eq 1). We verified that the piezos did indeed produce droplets of the desired size using Mie scattering techniques. A 1 W argon-ion laser operating at 488 nm was directed through the aerosol. The droplets in the aerosol scatter the laser light, and the resulting angular scattering intensity pattern is characteristic of the ratio of the droplet size to the incident wavelength. For each aerosol produced, the angular scattering pattern was measured with ~1° of angular resolution, and numeric non-linear-fit techniques were used in conjunction with Mie scattering theory to infer a droplet size distribution for the aerosol.

The droplet size distribution is well-peaked, and described by a log-normal function. We measured the peak of the size distribution to an accuracy of ~2%, and the size distribution typically has a width of ~20% of the peak size. The width of the distribution is a consequence of the atomization process. When the Faraday instability is more strongly driven-the condition under which we operate in order to produce a dense aerosol-the droplets are ejected from the fluid surface with a relatively larger size dispersion. A more narrow droplet size dispersion could be achieved at the expense of weaker driving and a less dense aerosol. In all comparisons between experiment and theory, we control for fluid temperature, as the piezo can deposit enough heat in the fluid sample to raise the local temperature by many degrees Celsius. A typical density of our aerosols is 5×10^6 droplets/cm^3.

We have measured the droplet distributions created by our atomization procedure over a wide range of fluid parameters, and thus establish the general viability of our technique for any fluid that can be atomized in the inviscid regime. For the vast majority of physical processes, atomization occurs in the inviscid regime, so this is not a very restrictive caveat.

As shown in Figure 1, following the aerosolization process, a pressure differential can be used to direct the aerosol into a heat pipe, where the temperature difference between the droplets and the surrounding environment causes the solvent to rapidly evaporate. For small droplets in a dry column of air, the Reynolds number is quite high, approximately 8×10^4, giving a time required for vapor diffusion on the order of 10^{-7} s for the experimental conditions used (16). Consequently, it can be assumed that the droplets are surrounded at all times by a completely dry layer, and there is no vapor layer present to inhibit further evaporation.

The rate of mass evaporation can then be related simply to the heat transferred to the droplets from the warmed air surrounding them

$$\frac{\partial m}{\partial t} = -\frac{hA\Delta T}{\lambda} \quad (2)$$

where A is the surface area of the droplet, ΔT is the temperature difference between the droplet and the surrounding environment, and λ is the latent heat of water (17). The heat transfer coefficient h can be calculated

$$h = \left(2 + 0.66\left(\frac{2R_d v\rho_a}{\mu_a}\right)^{0.5}\mathrm{Pr}^{1/3}\right)\left(\frac{K_d}{2R_d}\right) \quad (3)$$

where R_d is the radius of the droplet, v is the velocity of the droplets, ρ_a is the density of air, μ_a is the dynamic viscosity of air, and K_d is the thermal conductivity of water (16). Taking the droplets to be spherical and of uniform density, eqs 2 and 3 can be combined, giving the following expression

$$\frac{\partial m_d}{\partial t} = -\frac{4\pi\Delta T}{\lambda}\left(K_d\left(\frac{3m_d}{4\pi\rho_s}\right)^{1/3} + 0.66K_d\left(\frac{3v\rho_a m_d}{8\pi\rho_s\mu_a}\right)^{1/2}\mathrm{Pr}^{1/3}\right) \quad (4)$$

where ρ_s is the density of the solvent used and Pr is the Prandtl number. The difference in temperature between the droplet and its surroundings is therefore the dominant term in determining the rate of evaporation. The velocity at which the droplets travel through the evaporating chamber and the droplet mass also contribute to determining the evaporation rate, but as they are raised to the one-third power, a change in those variables has a relatively smaller effect.

The temperature used in eq 4 was assumed to be constant throughout the system. However, as the heat source is heat tape wound in a spiral across the outer surface of a copper pipe, the nonideal conductive ability of copper makes the center hotter than the extremities. Thus, the ΔT term is not constant, but rather a function of position in the pipe because of the temperature gradient introduced by the heating method. As a result,

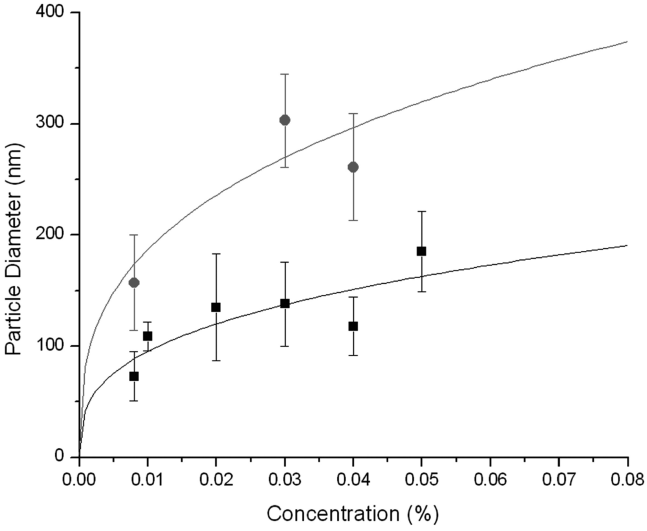

FIGURE 3. Chitosan nanoparticle diameter as a function of initial polymer concentration (% by weight) for the 6.6 MHz (squares) and 2.4 MHz (circles) oscillators. The bulk density was the only free parameter in the fit and was determined to be 185 ± 36 kg m^{-3}. The reduced χ^2 value for the fit is 0.63.

the temperature was measured near the extremities, where ΔT is smallest, so that an upper limit for the evaporation time is calculated.

Using eq 4, we controlled the temperature of the heat pipe, in order to ensure the solvent was evaporated from the droplets before reaching the slide chamber (Figure 1). This allowed the nanoparticles to be collected on silicon slides, and then sized using a scanning electron microscope. Imaging the slides provided visual confirmation that the particles were adequately dried, as their size would otherwise appear to be highly variable because of the wet particles spreading out upon impact.

To determine the size of the nanoparticles generated, a program was written in IgorPro to analyze images taken using the SEM. It detected nanoparticles based on a color threshold that could be set, and generated semimajor and semiminor axis averages and standard deviations. These averages were then used to approximate the nanoparticle diameters.

RESULTS AND DISCUSSION

As a proof of concept for our device, we chose chitosan to create chitosan nanoparticles. Chitosan is frequently the polymer of choice for use in drug and gene delivery. It exhibits low toxicity in cells, as well as a high level of biocompatibility and biodegradability, preventing it from accumulating in cells and tissues (18). Chitosan is also mucoadhesive and thus can affect several para- and intracellular pathways, promoting macromolecular uptake by epithelial cells (19−21). Properly formulated chitosans have been shown to bind effectively to DNA (22), as well as effectively deliver a variety of drugs with some cell specificity, including the anticancer drugs doxorubicin (23) and camptothecin (24).

Given the predictions of eq 1, the piezoelectric oscillator frequencies (MHz), and our desire to produce ∼100 nm chitosan particles, the slightly acidic aqueous chitosan solution concentrations were kept between 0.008 and 0.05% by weight. Further, for concentrations above 0.05%, the solutions became significantly more viscous, greatly reducing the number of droplets we could produce without exceeding the power limits of the piezo. To effectively dissolve the chitosan, the solution also contained 0.054% acetic acid and 0.09% sodium acetate, which maintained the pH at 4.5. The volatility of this buffer also minimized the risk of contamination in the nanoparticles produced (25).

One additional risk of using acetic acid buffers is that of ultrasonic wave-induced polymer degradation. Ultrasonic waves have previously been shown to degrade certain polymers, including chitosan, and this process is accelerated in acidic solvents (26, 27). However, most experiments show this is largely due to relatively low frequency waves (<1 MHz), or high power inputs (>1 KW) (28, 29). In our case, the power input was less than 0.06 W cm^{-3}, and as the pH was only mildly acidic, this process is unlikely to have had any effect on the polymer integrity or polydispersity.

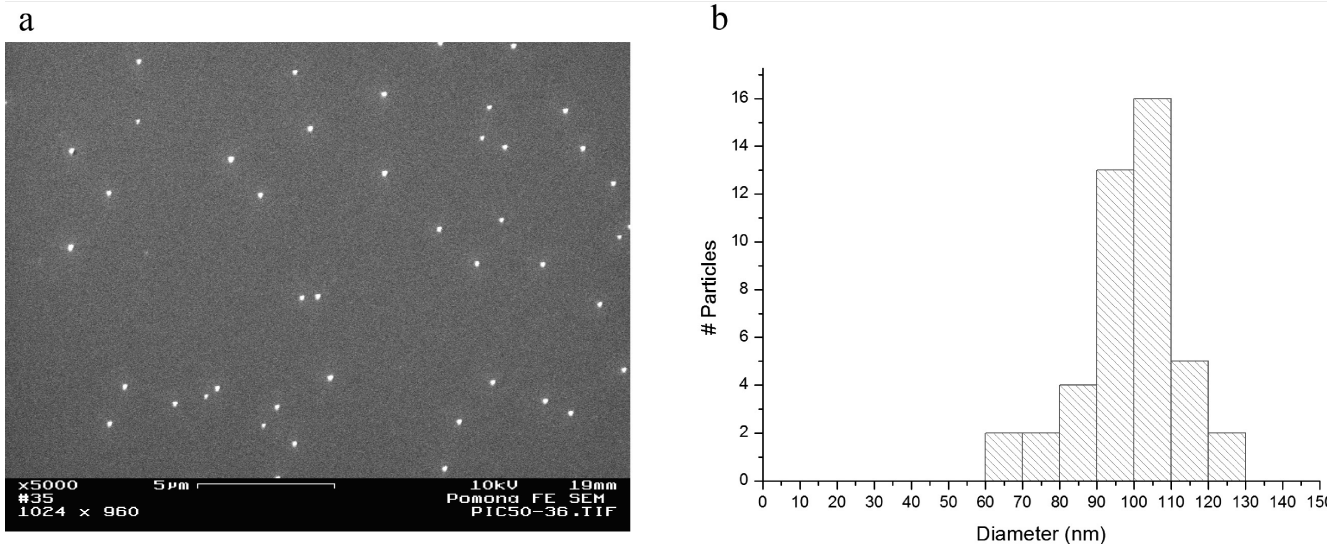

FIGURE 4. (a) Sample scanning electron microscope image of chitosan nanoparticles generated using the 6.6 MHz piezoelectric oscillator with a 0.01% chitosan solution. Using this image, along with zoomed in images of individual particles to improve sizing resolution, (b) a particle size distribution was generated. The average particle size on this slide was 98.6 ± 13 nm.

Using concentrations between 0.008 and 0.05%, sufficient amounts of dry nanoparticles were produced to allow for an accurate determination of their size. The mass density of the nanoparticles could not be determined experimentally, consequently this single parameter was fit empirically using eq 1, giving a value of 185 ± 36 kg m^{-3} (Figure 3). Using this value for the mass density, the measured nanoparticle sizes match well with our predicted sizes for both of the piezos used in our experiments. As expected, the higher frequency oscillator produced significantly smaller nanoparticles, and, in both cases, the particles increased in size when the concentration was increased. The average dispersion in nanoparticle diameter was 22%, which can be accounted for by the aerosolization process. As noted above, our atomization process produces droplets with an inherent distribution in diameter.

The chitosan used to prepare the solution had a bulk density between 180−300 kg m^{-3} and had a relatively high polydispersity of 1.6. As the bulk density determined from the fit matched quite closely to the original dry value, most of the solvent appears to have been successfully evaporated off. Though the polydispersity could have played a role in altering the particle sizes, even particles less than 100 nm in diameter were composed of several hundred polymer strands. Consequently, the polydispersity is unlikely to have had much of an effect, as the average polymer strand length in each droplet should be similar.

Figure 4a shows a scanning electron microscope image of the chitosan nanoparticles. The narrow size dispersion of the particles is evident in the figure. The nanoparticles are light enough that many were carried around the collection slides by the airflow, rather than impacting them. Our collection yield could be significantly improved by cooling the collecting slides, or building an electrostatic collection grid.

CONCLUSION

We can create narrowly dispersed chitosan nanoparticles in sizes ranging from 50−300 nm, with an average size dispersion of 22%, using an easily formulated chitosan solution. The size was controlled by both altering polymer solution concentrations and by changing the size of droplets formed from the solution. The size range we demonstrate can likely be expanded, using either higher frequency (smaller nanoparticles) or lower frequency (larger nanoparticles) piezos, so long as the piezos are capable of generating sufficient power to aerosolize the solutions.

Further study is needed to demonstrate the efficacy of this method to incorporate drugs or DNA. This combination should be possible by simply dissolving other compounds in the solution to be aerosolized; tight control of drug concentration in the nanoparticles would be established by careful control of the percent of drug in the solution. Moreover, this procedure can be extended to generate nanoparticles composed of different polymers, as long as they are soluble in a solvent that can be evaporated.

Acknowledgment. We thank David Tanenbaum, Dave Haley, and Pomona College, for the use of their scanning electron microscope, as well as Synedgen, Inc. for their support. We also thank Michael Maindi, Dustin McCarren, and Steven Pankratz for their help. This work was supported by the National Science Foundation under Grants PHY-0456898 and PHY-0757989, and acknowledgment is made to the Donors of the Petroleum Research Fund administered by the American Chemical Society for partial support of this research.

REFERENCES AND NOTES

(1) Liong, M.; Lu, J.; Kovochich, M.; Xia, T.; Ruehm, S.; Nel, A.; Tamanoi, F.; Zink, J. *ACS Nano* **2008**, *2*, 889–896.
(2) Chan, C. Applying Optical Coherence Microscopy to Frog and Fruit Fly Embriogenesis. Senior Thesis, Harvey Mudd College, Claremont, CA, 2008.
(3) Kaplitt, M.; Feigin, A.; Tang, C.; Fitzsimons, H.; Mattis, P.; Lawlor, P.; Bland, R.; Young, D.; Strybing, K.; Eidelberg, D.; During, M. *Lancet* **2007**, *369*, 2097–2105.
(4) Somia, N.; Verma, I. *Nat. Rev. Genet.* **2000**, *1*, 91–99.
(5) Prabha, S.; Zhou, W.; Panyam, J.; Labhasetwar, V. *Int. J. Pharm.* **2002**, *244*, 105–115.
(6) Moghimi, S.; Hunter, A.; Murray, J. *Pharmacol. Rev.* **2001**, *53*, 283–318.
(7) Soppimath, K.; Aminabhavi, T.; Kulkarni, A.; Rudzinski, W. *J. Controlled Release* **2001**, *70*, 1–20.
(8) Panyam, J.; Labhasetwar, V. *Adv. Drug Delivery Rev.* **2003**, *55*, 329–347.
(9) Nagarwal, C.; Kant, S.; Singh, P.; Maiti, P.; Pandit, J. *J. Controlled Release* **2009**, *136*, 2–13.
(10) Csaba, N.; Garcia-Fuentes, M.; Alonso, M. *Adv. Drug Delivery Rev.* **2009**, *61*, 140–157.
(11) Kumar, M. *J. Pharm. Pharm. Sci.* **2000**, *3*, 234–258.
(12) Uhrich, K.; Cannizzaro, S.; Langer, R.; Shakesheff, K. *Chem. Rev.* **1999**, *99*, 3181–3198.
(13) Agnihotri, S.; Mallikarjuna, N.; Aminabhavi, T. *J. Controlled Release* **2004**, *100*, 5–28.
(14) Donnelly, T. D.; Hogan, J.; Mugler, A.; Schubmehl, M.; Schommer, N.; Bernoff, A. J.; Forrest, B. *Phys. Fluids* **2004**, *16*, 2843.
(15) Donnelly, T. D.; Hogan, J.; Mugler, A.; Schubmehl, M.; Schommer, N.; Bernoff, A. J.; Dasnurkar, S.; Ditmire, T. *Rev. Sci. Instrum.* **2005**, *76*, 113301.
(16) Sazhin, S. *Prog. Energy Combust. Sci.* **2006**, *32*, 162–214.
(17) Evstropova, E. V.; Osiptsov, A. N.; Shapiro, E. G. *Fluid Dynamics* **1992**, *27*, 331–337.
(18) De Salamanca, A.; Diebold, Y.; Calonge, M.; García-Vazquez, C.; Callejo, S.; Vila, A.; Alonso, M. *Invest. Ophthalmol. Vis. Sci.* **2006**, *47*, 1416–1425.
(19) Dodane, V.; Khan, M.; Merwin, J. *Int. J. Pharm.* **1999**, *182*, 21–32.
(20) Grenha, A.; Grainger, C.; Dailey, L.; Seijo, B.; Martin, G.; Remuñán-López, C.; Forbes, B. *Eur. J. Pharm. Sci.* **2007**, *31*, 73–84.
(21) Fernández-Urrusuno, R.; Calvo, P.; Remuñán-López, C.; Vila-Jato, J.; Alonso, M. *Pharm. Res.* **1999**, *16*, 1576–1581.
(22) Mao, H.; Roy, K.; Troung-Le, V.; Janes, K.; Lin, K.; Wang, Y.; August, J.; Leong, K. *J. Controlled Release* **2001**, *70*, 399–421.
(23) Janes, K.; Fresneau, M.; Marazuela, A.; Fabra, A.; Alonso, M. *J. Controlled Release* **2001**, *73*, 255–267.
(24) Min, K.; Park, K.; Kim, Y.; Bae, S.; Lee, S.; Jo, H.; Park, R.; Kim, I.; Jeong, S.; Kim, K.; Kwon, I. *J. Controlled Release* **2008**, *127*, 208–218.
(25) Wang, X. *J. Membr. Sci.* **2000**, *170*, 71–79.
(26) Mason, T.; Lorimer, J. *Applied Sonochemistry: Uses of Power Ultrasound in Chemistry and Processing*; Wiley VCH: Weinheim, Germany, 2002; pp 161−171.
(27) Chen, R.; Chang, J. R.; Shyur, J. *Carbohyd. Res.* **1997**, *299*, 287–294.
(28) Kost, J.; Leong, K.; Langer, R. *Proc. Natl. Acad. Sci. U.S.A.* **1989**, *86*, 7663–7666.
(29) Liu, H.; Bao, J.; Du, Y.; Zhou, X.; Kennedy, J. *Carbohyd. Polym.* **2006**, *64*, 553–559.

AM100375W